PAPER

Check for updates

Continuous selective deoxygenation of palm oil for renewable diesel production over Ni catalysts supported on Al_2O_3 and La_2O_3–Al_2O_3†

Kyriakos N. Papageridis, [ID] [a] Nikolaos D. Charisiou, [ID] [a] Savvas Douvartzides,[ab] Victor Sebastian, [ID] [cde] Steven J. Hinder,[f] Mark A. Baker,[f] Ayesha A. AlKhoori,[g] Sara I. AlKhoori,[g] Kyriaki Polychronopoulou [ID] [gh] and Maria A. Goula [ID] *[a]

The present study provides, for the first time in the literature, a comparative assessment of the catalytic performance of Ni catalysts supported on γ-Al_2O_3 and γ-Al_2O_3 modified with La_2O_3, in a continuous flow trickle bed reactor, for the selective deoxygenation of palm oil. The catalysts were prepared *via* the wet impregnation method and were characterized, after calcination and/or reduction, by N_2 adsorption/ desorption, XRD, NH_3-TPD, CO_2-TPD, H_2-TPR, H_2-TPD, XPS and TEM, and after the time-on-stream tests, by TGA, TPO, Raman and TEM. Catalytic experiments were performed between 300–400 °C, at a constant pressure (30 bar) and different LHSV (1.2–3.6 h^{-1}). The results show that the incorporation of La_2O_3 in the Al_2O_3 support increased the Ni surface atomic concentration (XPS), affected the nature and abundance of surface basicity (CO_2-TPD), and despite leading to a drop in surface acidity (NH_3-TPD), the Ni/LaAl catalyst presented a larger population of medium-strength acid sites. These characteristics helped promote the SDO process and prevented extended cracking and the formation of coke. Thus, higher triglyceride conversions and n-C_{15} to n-C_{18} hydrocarbon yields were achieved with the Ni/LaAl at lower reaction temperatures. Moreover, the Ni/LaAl catalyst was considerably more stable during 20 h of time-on-stream. Examination of the spent catalysts revealed that both carbon deposition and degree of graphitization of the surface coke, as well as, the extent of sintering were lower on the Ni/LaAl catalyst, explaining its excellent performance during time-on-stream.

1 Introduction

Over the last decades world energy consumption has dramatically increased due to the growth in population and economic output, especially in emerging market economies, leaving fossil

[a] *Laboratory of Alternative Fuels and Environmental Catalysis (LAFEC), Department of Chemical Engineering, University of Western Macedonia, GR-50100, Greece. E-mail: mgoula@uowm.gr; Tel: +30 24610 68296*

[b] *Department of Mechanical Engineering, University of Western Macedonia, GR-50100, Greece*

[c] *Department of Chemical Engineering and Environmental Technology, Universidad de Zaragoza, Campus Río Ebro-Edificio I + D, 50018 Zaragoza, Spain*

[d] *Instituto de Nanociencia y Materiales de Aragón (INMA), Universidad de Zaragoza-CSIC, c/María de Luna 3, 50018 Zaragoza, Spain*

[e] *Networking Research Center on Bioengineering, Biomaterials and Nanomedicine, CIBERBBN, 28029 Madrid, Spain*

[f] *The Surface Analysis Laboratory, Faculty of Engineering and Physical Sciences, University of Surrey, Guildford, GU2 4DL, UK*

[g] *Department of Mechanical Engineering, Khalifa University of Science and Technology, P.O. Box 127788, Abu Dhabi, United Arab Emirates*
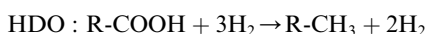
[h] *Center for Catalysis and Separations, Khalifa University of Science and Technology, P.O. Box 127788, Abu Dhabi, United Arab Emirates*

† Electronic supplementary information (ESI) available. See DOI: 10.1039/d0ra08541c

fuel reserves depleted. Moreover, there is almost unanimous agreement amongst the scientific community that the increase in the concentration of greenhouse gases (GHG) into the atmosphere leads to climate change at a scale that threatens the very survival of the biosphere, including the human species.[1–3] One way to reduce CO_2 emissions is to replace petro-based sources in transportation with biofuels, as the sector uses nearly 40% of global primary energy.[4]

An important renewable resource for the production of green liquid fuels are triglycerides, which consist of C_8–C_{24} fatty acids, the main components of vegetable oils and animal fats; these are usually used for the production of biodiesel, a mixture of Fatty Acids Methyl Esters (FAMEs). However, biodiesel has a number of important disadvantages, in comparison to petroleum diesel, such as low thermal and oxidation stability (due to its high oxygen content), low heating value, high viscosity and poor cold weather performance.[5] Moreover, the process also results in the production of large amounts of crude glycerol as byproduct, which at the moment is considered an industrial waste, despite intense efforts at developing processes that will utilize it.[6,7] Therefore, the development of technologies that overcome the disadvantages associated with the production and use of biodiesel are of great interest.
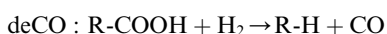
Selective catalytic deoxygenation (SDO) of triglycerides is a process that produces a mixture of C_{15}–C_{18} normal and isomer paraffins, also called "renewable diesel", "green diesel" or "bio-hydrogenated diesel (BHD)", which has chemical resemblance to that of conventional petroleum diesel. As a result, green diesel provides better diesel properties in comparison to biodiesel, such as high cetane number, high energy density, very low sulfur content and since it does not contain oxygen, it is non-corrosive, more stable and it can be used in neat or blend form.[8–12]

The SDO of triglycerides involves three different reactions, which are commonly known as hydrodeoxygenation (HDO), decarbonylation (deCO) and decarboxylation (deCO$_2$). HDO (1) is an exothermic reaction, which leads to a saturated hydrocarbon product that has the same number of carbon atoms as the corresponding fatty acid bound in the triglyceride, as oxygen is removed in the form of H_2O molecules. However, while HDO is highly selective to diesel-like hydrocarbons it also requires high H_2 pressures (mostly available only in centralized facilities), and the use of sulfated catalysts (which can contaminate the final product with sulfur). On the other hand, deCO (2a) and (2b) and deCO$_2$ (3) are mildly endothermic reactions that produce a saturated hydrocarbon product with one carbon atom less than the corresponding fatty acid bound in the triglyceride, as oxygen is removed in the form of CO and CO_2, respectively. The deCO and deCO$_2$ reactions are quite difficult to distinguish, as CO_2 and CO react with H_2 on the surface of the catalyst. Therefore, these routes are commonly known as deCO$_x$ reactions.[13–16]
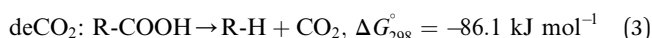
$$\text{HDO}: \text{R-COOH} + 3H_2 \rightarrow \text{R-CH}_3 + 2H_2O, \Delta G^{\circ}_{298} = -83.5 \text{ kJ mol}^{-1} \quad (1)$$

$$\text{deCO}: \text{R-COOH} + H_2 \rightarrow \text{R-H} + CO + H_2O, \Delta G^{\circ}_{298} = -17 \text{ kJ mol}^{-1} \quad (2a)$$

$$\text{deCO}: \text{R-COOH} \rightarrow \text{R-H} + CO + H_2O, \Delta G^{\circ}_{298} = -67.6 \text{ kJ mol}^{-1} \quad (2b)$$

$$\text{deCO}_2: \text{R-COOH} \rightarrow \text{R-H} + CO_2, \Delta G^{\circ}_{298} = -86.1 \text{ kJ mol}^{-1} \quad (3)$$

where R is a saturated alkyl group and R′ is an unsaturated alkyl group.

Most of the studies in the literature have focused on the development of noble metal catalysts, such as Pt, Pd, Ru and Rh, supported on high surface area carriers, as such systems are known to exhibit high activity and selectivity to deCO$_x$ reactions.[17–28] However, despite their high catalytic performance, noble metals are sensitive to a small number of oxygenated compounds present in the feedstock. Moreover, noble metals are considered expensive for large scale applications. Therefore, recent research focuses on the development of low cost, transition metal catalysts based on Ni, Cu and Co, that have been shown to exhibit comparable catalytic performance to those of precious metals in the deCO$_x$ of triglycerides. For example, Veriansyah et al.[27] studied the effects of six different types of

metal supported catalysts on the deoxygenation of soybean oil to produce renewable diesel. The experiments were carried out in a high-pressure batch reactor at 400 °C, with an H_2 pressure of 92 bar. The authors showed that for a catalyst/oil weight ratio of 0.044 deoxygenation activity decreased in the order of NiMo/γ-Al$_2$O$_3$ > Pd/γ-Al$_2$O$_3$ > CoMo/γ-Al$_2$O$_3$ > Ni/SiO$_2$–Al$_2$O$_3$ > Pt/γ-Al$_2$O$_3$ > Ru/γ-Al$_2$O$_3$. Similarly, Morgan et al.[28] examined the conversion of triglycerides (tristearin and triolein) to diesel-like hydrocarbons in a batch reactor at 350 °C and 7 bar and showed that the deoxygenation activity followed the order Ni/C > Pt/C > Pd/C. Moreover, the Ni/C catalyst provided the higher C_8–C_{17} product yield.

Alumina is a ubiquitous supporting material for a variety of catalytic reactions, due to its high specific surface area (which improves metal dispersion) and high thermal stability under reaction conditions.[29–36] Moreover, as it is mildly acidic, a property that is considered beneficial in catalysts used for the deoxygenation of triglycerides, it has been used extensively in catalytic systems tested in the SDO process. An excellent work was provided by Gousi et al.,[36] which screened Ni catalysts with loading in the range of 0–100 wt%, in a semi-batch reactor at 310 °C, 40 bar and volume of oil (mL)/mass of catalyst (g) ratio equal to 100, and observed that both the conversion of sunflower oil and the yield of hydrocarbons maximize at Ni about 60 wt%. The initial increase of the conversion up to the critical metal loading of 60 wt% was attributed to the increase of the metal active phase with a simultaneous decrease of the amount of an inactive NiAl$_2$O$_4$-like phase. The subsequent fall of the deoxygenation rate at higher metal loadings was attributed to the competitive decrease of the specific surface area. The authors also reported that the main liquid products consisted primarily of n-C_{15} to n-C_{18}, intermediate fatty acids and esters. However, alumina is also known to induce the deposition of carbon, which inevitably, leads to catalyst deactivation. For the SDO, the formation of coke deposits on Ni/Al$_2$O$_3$ systems has been associated with the ability of Ni to promote the cracking reaction and the acidity of the γ-Al$_2$O$_3$ support.[37]

Catalyst deactivation and/or improved performance in Ni catalyzed reactions are commonly addressed by the addition of modifiers. In some of our previous works, we confirmed that the incorporation of La$_2$O$_3$ in an Al$_2$O$_3$ support improves the dispersion of the active species, strengthens the interactions between active phase and support, increases the basic sites of the catalyst and redistributes the acid sites in terms of strength and density; as a result, considerably improved catalytic performance was observed.[38,39] However, to the best of our knowledge, the use of Ni/La$_2$O$_3$–Al$_2$O$_3$ catalysts in the deoxygenation of palm oil in trickle bed reactors has never been reported in the literature.

In fact, searching through the relevant literature, it becomes obvious that although one may find a small number of research studies for the SDO of model compounds in trickle bed reactors,[9,37,40,41] studies involving triglycerides, such as palm oil, are almost nonexistent. However, there is an obvious need to move into trickle bed reactors using oil feedstocks, as such systems allow the evaluation of catalytic stability during long term time-on-stream tests, a necessary part of scaling up the process. Amongst the handful of available works, mention should be

made to the group of Faungnawakij for the works presented in ref. 9 and 40. In the first of these works,[9] the authors studied the production of renewable diesel *via* the deoxygenation of refined palm oil in a trickle bed reactor using Co, Ni, Pd and Pt monometallic catalysts supported on γ-Al_2O_3, prepared by the incipient wetness impregnation method. Deoxygenation tests were conducted at 330 °C, H_2 pressure of 50 bar, liquid hourly space velocity (LHSV) of 1 h^{-1} and H_2/oil feed ratio of 1000 cm^3 cm^{-3}. The authors reported that catalytic activity decreased in the order of Co (88%) > Pd (85%) > Pt (80%) > Ni (70%) and that Ni, Pd and Pt catalysts were more selective to the deCO reaction pathway, whereas the Co catalyst was selective for both $deCO_x$ and HDO reaction pathways. In the second work,[40] the authors studied the deactivation and regeneration behavior of Ni and Co catalysts supported on γ-Al_2O_3 during the hydrodeoxygenation of palm oil and concluded that the main reason for catalyst deactivation, after 150 h of time-on-stream, was carbon deposition; sintering only played a minor role.

In view of the foregoing, the present study investigated the effect of hydrotreating temperature and LHSV on the catalytic performance of Ni catalysts supported on γ-Al_2O_3 and γ-Al_2O_3 modified with La_2O_3, in a continuous flow trickle bed reactor, for the selective deoxygenation of palm oil. The catalysts were prepared *via* the wet impregnation method, at a constant metal loading of 8 wt%. The catalytic samples, after calcination and/or reduction, were characterized by N_2 adsorption/desorption, XRD, NH_3-TPD, CO_2-TPD, H_2-TPR, H_2-TPD, XPS and TEM, in order to provide an insight into the effect on performance by their physical and chemical properties. Moreover, the spent catalysts after 20 h of time-on-stream tests were characterized by TGA, TPO, Raman and TEM, in order to determine the extent of carbon deposition and metal particle sintering on the spent samples.

2 Materials and methods

2.1 Reagents and feedstock

The analysis of the liquid products of the reaction necessitated the use of a number of high quality chemical reagents (detailed information regarding chemical grades can be found in ref. 42), *i.e.*, linoleic acid, palmitic acid, oleic acid, stearic acid, tridecane, cyclohexanone, a mixture of 37 fatty acid methyl esters (all Sigma-Aldrich), heptane, dodecane, cyclohexane, chloroform (all Honeywell) and a calibration sample kit #2 for n-C_8 to n-C_{18} alkanes (Agilent Technologies). The main components of the palm oil used as feed are presented in Table 1.

Table 1 Fatty acid composition of the palm oil

Fatty acid	Structure	Formula	Composition, wt%
Myristic acid	$C_{14:0}$	$C_{14}H_{28}O_2$	0.90
Palmitic acid	$C_{16:0}$	$C_{16}H_{32}O_2$	41.60
Palmitoleic acid	$C_{16:1}$	$C_{16}H_{30}O_2$	0.70
Stearic acid	$C_{18:0}$	$C_{18}H_{36}O_2$	2.10
Oleic acid	$C_{18:1}$	$C_{18}H_{34}O_2$	43.90
Linoleic acid	$C_{18:2}$	$C_{18}H_{32}O_2$	10.40
Linolenic acid	$C_{18:3}$	$C_{18}H_{30}O_2$	0.40

2.2 Catalysts preparation

The properties of the commercially available alumina (Akzo) and lanthana–alumina (4 wt% La_2O_3, W.R. Grace, MI-386) supports used herein can be found in ref. 38 and 39. The Ni based catalysts used in the present work were prepared *via* the wet impregnation method. In brief, prior to catalyst synthesis, the γ-Al_2O_3 support was crushed and sieved to particles with sizes between 350 and 500 μm. The La_2O_3–Al_2O_3 support was first pelletized and then crushed/sieved to the same size. Both supports were air-dried overnight at 120 °C and calcined at 400 °C for 4 h under an atmosphere of air. Thereafter, the impregnation solutions were prepared using calculated amounts of $Ni(NO_3)_2 \cdot 6H_2O$ ($\geq$97%, Fluka), dissolved in distilled and de-ionized water in order to obtain final catalysts of 8 wt% Ni loading. The resulting slurries were evaporated using a rotary evaporator at 70 °C for 6 h, dried at 120 °C for 12 h and finally calcined at 400 °C for 4 h. These samples will be hereafter denoted as Ni/Al and Ni/LaAl catalysts.

2.3 Catalysts characterization

The specific surface area (SSA), pore volume (V_p) and pore size distribution (PSD) was investigated using a high-resolution porosimeter (3Flex Micromeritics). The SSA was determined by the multi-point Brunauer–Emmett–Teller (BET) method in the relative pressure range $0.05 < P/P_0 < 0.20$, while PSD was calculated by the BJH Theory.

The total metal loading (wt%) of the catalysts was determined by Inductively Coupled Plasma Atomic Emission Spectroscopy (ICP-AES-on a Perkin-Elmer Optima 4300DV apparatus). The detailed methodology used has been described previously.[43]

The X-ray diffraction (XRD) profiles of the catalytic samples were obtained using a ThermoAl diffractometer system at 40 kV and 30 mA, with Cu Kα radiation source (λ = 0.15178 nm). The diffraction patterns were recorded between Bragg angles (2θ) 2°–70°, at a scanning rate of 0.04° per 1.2 min.

The acidity and basicity of the catalytic samples was determined using NH_3 and CO_2 temperature-programmed desorption (NH_3-/CO_2-TPD) experiments. Catalyst reducibility and the strength of Ni–support interaction were studied using H_2 temperature-programmed reduction (H_2-TPR). The NH_3-/CO_2-TPD and H_2-TPR experiments were conducted on an Autochem 2920 Micromeritics. H_2-TPD experiments were performed in a quartz fixed-bed reactor. The precise methodology used can be found in the ESI accompanying ref. 42. The H_2 signal (m/z = 2) was continuously monitored with an on-line mass spectrometer (QMS 200 Prisma Quadrupole Mass Spectrometer) and converted into concentration (ppm).

The oxidation state and atomic composition of the catalysts were studied by X-ray photoelectron spectroscopy (XPS) using a ThermoFisher Scientific Instruments K-Alpha+ spectrometer. The XPS spectra were recorded using a monochromated Al Kα X-ray source ($h\nu$ = 1486.6 eV).

Transmission electron microscopy (TEM) observations on the reduced and spent catalysts were carried out using a 200 kV G2 20 S-Twin Tecnai microscope with a LaB6 electron source fitted with a "SuperTwin®" objective lens allowing a point-to-point resolution of 2.4 Å.

Apart from electron microscopy, the coke deposited on the spent catalytic samples was characterized by: (a) Raman spectroscopy using a Witec Alpha 300 instrument, equipped with 532 nm laser and research grade optical microscope with various lenses. The instrument features a manual sample positioning with both planar (x,y-direction) and depth scans (z-direction). All the catalysts spectra were acquired using single-point Raman spectrum acquisition. (b) Temperature Programmed Oxidation (TPO), using Autochem 2920 unit under a 20% O_2/He gas atmosphere. (c) Thermogravimetric analysis (TGA) carried out using a Leco TGA701. In the procedure, 100 mg of the spent catalyst were subjected to TGA scan from room temperature to 1000 °C at a heating rate of 10 °C min^{-1} under a flow of dry air (3.5 L min^{-1}). Curie point standards were utilized for the temperature calibration.

2.4 Catalysts evaluation

2.4.1 Catalysts testing.
Catalytic testing was carried out using a continuous flow, fixed bed, tubular stainless steel reactor (BTRS-Jr Autoclave Engineers, USA) with an internal diameter of 0.7 cm, length of 30 cm and volume of 12 mL (Fig. 1). The system used and the experimental procedure followed has been described in detail in ref. 42, thus only a short summary is provided in this section.

Prior to performing any catalytic reaction measurement, a specific amount of catalyst (held in place using quartz wool) was *in situ* activated by flowing 50 mL min^{-1} of H_2 (99.999 v/v%) in atmospheric pressure, at 400 °C, for 2 h. Following activation, the catalyst was purged under a flow of 100 mL min^{-1} of Ar (99.999 v/v%), the system was set to the desired reaction temperature and pressure and the reaction feed was introduced into the catalyst bed along with a flow of H_2. The liquid stream of the palm oil dissolved in dodecane (5 wt%), which was kept under continuous stirring at room temperature, was introduced to the system at a rate of 0.2 mL min^{-1}. In order to ensure

operation at steady state conditions, the first measurement was taken after the feed had passed for approximately 80 min through the catalyst bed. In addition, a non-catalytic experiment (blank experiment) was carried out at 375 °C, 30 bar, 1.2 h^{-1} and 1000 cm^3 (cm^3)$^{-1}$ in order to assess the extent of non-catalytic (as opposed to catalytic) contributions to diesel-like hydrocarbons and fatty acids yield. The liquid products were manually collected from the gas–liquid separator while the gaseous products were sent to a gas chromatograph (GC).

The selective deoxygenation of palm oil was carried out using two different sets of experiments. During the first set of experiments (experimental protocol #1) the liquid and gaseous product composition was investigated during short time-on-stream tests (6 h) as follows: (a) at temperatures between 300–400 °C, and (b) at LHSV between 1.2–3.6 h^{-1} (for comparison purposes, all other parameters were kept constant). Experimental protocol #2 aimed at investigating the stability of the catalysts during long-term stability tests (20 h) at 375 °C and LHSV = 1.2 h^{-1} (as these were identified as the optimal conditions during experimental protocol #1). For both protocols, the H_2 pressure and the H_2/oil ratio were kept constant at 30 bar and 1000 cm^3 (cm^3)$^{-1}$, respectively. During the short time stability tests liquid and gaseous products were analyzed at 1 h intervals. For the long stability tests, liquid effluents were analyzed every 4 h and gaseous products every 1 h.

2.4.2 Product analysis.
The gas products were analyzed online by an Agilent 7890A Gas Chromatograph (GC) equipped with TCD and FID detectors and two capillary columns connected in series HP-Plot-Q (19095-Q04, 30 m length, 0.530 mm I.D.) and HP-Molesieve (19095P-MSO, 30 m length, 0.530 mm I.D.). The main components of the gas products were H_2, CO, CO_2, CH_4; trace amounts of C_2H_6 and C_3H_8 were also detected but not quantified.

The liquid products were analyzed offline by an Agilent 7890A/5975C Triple-Axis Detector diffusion pump Gas Chromatographer-Mass Spectrometer (GC-MS), equipped with an Agilent Multimode inlet and an Agilent 7683B Automatic Liquid Sampler. The multimode inlet, containing a deactivated open ended helix liner (Agilent Technologies), was operated in a split ratio of 25 : 1, split flow rate of 50 mL min^{-1} and a temperature of 300 °C which was maintained for the duration of the analysis.

The methodology used for the analysis of the liquid products, followed closely the one reported by Santillan-Jimenez *et al.*[13,14] and Lercher *et al.* in ref. 44, and has been provided in detail in ref. 42.

2.4.3 Reaction metrics.
Mole balance of the organic liquid products was used to evaluate the catalytic performance in terms of palm oil conversion, n-C_{15} to n-C_{18} product yields and % contributions of the hydrodeoxygenation (HDO %) and decarbonylation/decarboxylation (deCO/deCO$_2$ %) reactions. For all experimental conditions the mole balance was greater than 94%. Performance parameters were calculated using the following eqn (4)–(7):
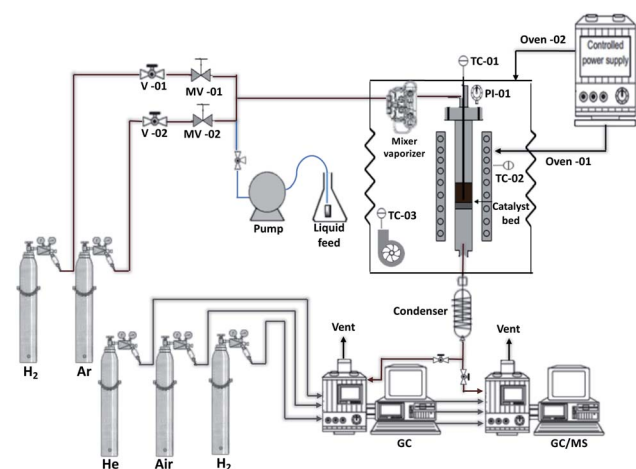

Fig. 1 Schematic flow chart of the experimental setup for catalytic testing (V = Valve, MV = Metering Valve, TC = Temperature Controller, PI = Pressure Indicator, GC = Gas Chromatographer, MS = Mass Spectrometer).

$$X(\text{mol\%}) = \frac{\text{mol TG in feed} - \text{mol TG in product}}{\text{mol TG in feed}} \times 100 \quad (4)$$

$$Y(C_{15} - C_{18})(\text{mol}\%) = \frac{\text{mol of } n\text{-}C_{15} \text{ to } n\text{-}C_{18}}{\text{mol of } C_{16} \text{ and } C_{18} \text{ fatty acid}} \times 100 \quad (5)$$

$$\text{HDO}(\text{mol}\%) = \frac{\text{mol of } n\text{-}C_{16} \text{ and } n\text{-}C_{18}}{\text{mol of } C_{16} \text{ and } C_{18} \text{ fatty acid}} \times 100 \quad (6)$$

$$\text{deCO/deCO}_2(\text{mol}\%) = \frac{\text{mol of } n\text{-}C_{15} \text{ and } n\text{-}C_{17}}{\text{mol of } C_{16} \text{ and } C_{18} \text{ fatty acid}} \times 100 \quad (7)$$

3 Results and discussion

3.1 Catalysts characterization

It is noted that additional information regarding the characterization of the catalysts using N_2 adsorption/desorption, ICP-AES, XRD, H_2-TPD and XPS can be found in the ESI.†

Elemental analysis (ICP-AES) carried out on the calcined catalysts showed that the desired Ni loading was achieved for both as it was found equal to 7.83 wt% for the Ni/Al and 7.92 wt% for the Ni/LaAl. Fig. S1a and b† presents the adsorption–desorption isotherms obtained for the calcined Ni/Al and Ni/LaAl catalysts. Both have relatively similar specific surface areas (SSA) and pore volumes *i.e.*, 158.5 $m^2 g^{-1}$ and 0.44 $cm^3 g^{-1}$ for the Ni/Al and 142.2 $m^2 g^{-1}$ and 0.55 $cm^3 g^{-1}$ for the Ni/LaAl.

Fig. 2 presents the X-ray diffractograms of the reduced Ni/Al and Ni/LaAl catalysts. The characteristic peaks of NiO at 37° and 43° and Ni^0 at 44° and 51° can be barely traced. So as expected, a mixture of metallic Ni^0 and NiO are present in the catalyst. Fig. S1c† presents the corresponding X-ray diffractograms for the calcined Ni/Al and Ni/LaAl catalysts.

The number and strength of basic sites present on the calcined Ni/Al and Ni/LaAl catalysts were investigated through CO_2-TPD experiments (Fig. 3a). The experiments were carried out at room temperature (25 °C), after pre-treatment in reducing atmosphere. According to the literature,[45,46] the basic sites can be categorized according to their strength, in relation with the CO_2 temperature desorption peaks as: (i) weak (50–200 °C), (ii)

intermediate (200–400 °C), and (iii) strong (400–650 °C). From the results presented herein, the Ni/Al catalyst presents three well defined peaks; thus, these can be linked to the presence of weak, medium and strong basic sites, respectively. On the other hand, the CO_2-TPD profile of the Ni/LaAl catalyst shows three well resolved CO_2 desorption peaks, as the Ni/Al, but rather shifted to higher temperatures. This dictates that La addition strengthens the basic sites. The desorption peaks at the highest temperature regime can be linked to the thermal decomposition of La-carbonates, respectively.[47] It is worth pointing out that the modification of γ-Al_2O_3 support with La_2O_3 alters significantly the nature of the surface basicity (shift to higher temperature), as well as their abundance; the concentration of the basic sites was found for the Ni/Al and Ni/LaAl to be 34.2 and 47 mmol CO_2 per g_{cat}, respectively. Also, the density of the basic sites is 0.216 and 0.33 mmol CO_2 per g_{cat}. Wierzbicki *et al.*[48] reported that weak, medium and strong basic sites are assigned to the surface OH^- groups, to the Lewis acid-base pairings and to the surface O^{2-} species at low-coordination environment, respectively.

The acidity of the Ni/Al and Ni/LaAl catalysts were examined using NH_3-TPD measurements. As can be observed from Fig. 3b, the Ni/Al and Ni/LaAl catalysts are dominated by three
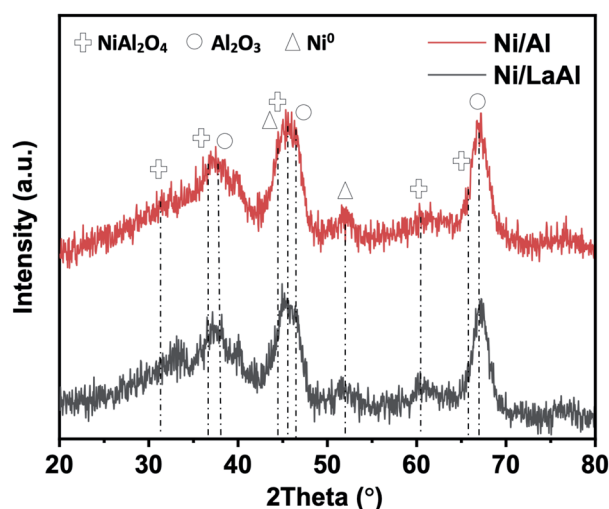

Fig. 3 (a) CO_2-TPD, and (b) NH_3-TPD profiles obtained over the Ni/Al and Ni/LaAl catalysts.

Fig. 2 XRD patterns of the reduced Ni/Al and Ni/LaAl catalysts.

desorption regions; the first is located at temperatures lower than 200 °C, the second at medium desorption temperatures (200–500 °C), and the third at temperatures higher than 500 °C. These desorption areas can be assigned to weak, medium and strong acid sites,[45,46] whereas the low temperature peak can be partially assigned to the physisorbed ammonia. The peaks detected at temperatures higher than 500 °C may partially correspond to NO_x species being produced as a result of NH_3 reaction with the oxygen species of the catalyst. From the NH_3-TPD profiles of the catalytic materials tested herein, both catalysts present mostly weak acid sites, while the modification of γ-Al_2O_3 support with the introduction of La_2O_3 led to a drop in surface acidity from 200 mmol g_{cat}^{-1} (Ni/Al) to 170 mmol g_{cat}^{-1} (Ni/LaAl). Also, the density of the acid sites is 1.26 and 1.19 mmol NH_3 per m^2 for Ni/Al and Ni/LaAl, respectively. Though the Ni/LaAl catalyst has a distinct peak at 400 °C (medium strength acid sites). This is of great interest for the reaction under investigation, as mildly acidic catalytic materials promote the SDO process and prevent extending cracking and the formation of coke. The results of the NH_3-TPD profile of the Ni/Al catalyst are in line with the findings reported from Li et al.[49]

The reducibility behavior of the Ni/Al and the Ni/LaAl catalysts and the degree of interaction of Ni species with the support were studied using H_2-TPR studies (Fig. 4). It is generally accepted that the reduction of NiO weakly interacting with the support takes places at temperatures lower than 500 °C, while the reduction of NiO strongly interacting with the bulk of the support takes place over this temperature.[50,51] Kathiraser et al.,[52] using La-modified Ni/Al_2O_3 catalysts for the CO_2 reforming of CH_4, reported that the TPR peaks in the 300–500 °C range can be linked to free and amorphous NiO phase, respectively, whereas the peaks in the 500–650 °C range correspond to the reduction of the mixed Ni-support phase towards metallic Ni. As can be observed from Fig. 4, and for both the Ni/Al and Ni/LaAl catalysts, the main reduction peak of the NiO species is in the 300–650 °C region, in good agreement with the H_2-TPR

reduction behavior of similar catalysts found in the literature.[49,52,53] However, it is noted that in the case of the Ni/LaAl catalyst there is an additional peak around 220 °C which supports the fact that the modification of alumina using La_2O_3 facilitated the reduction of the Ni species and most likely led to polydispersion of NiO species (in terms of particle size) that are in different electronic interaction with the support. According to the histogram results (based on the TEM studies) the size distribution is between 2–10 nm. This is in agreement with the inability to trace Ni or NiO using XRD. It is also worth noticing that in the H_2-TPR the different species of Ni or NiO are monitored not only in relation to their size but also in relation to their geometrical location with respect to the support; the latter dictates the extend of Ni or NiO interaction with the support. For instance, it is possible to get two different peaks for small crystallites of Ni at low and high temperature corresponding to weak and strong Ni–support interactions. This increases the polydispersity that was measured using the H_2-TPR technique.

The strength of H_2 interaction with the Ni centers, as well as, the amount of chemisorbed H_2 were investigated by H_2-TPD experiments; these were carried out on the reduced Ni/Al and Ni/LaAl catalysts. As can be observed from the profiles obtained (Fig. S2†), the Ni/Al catalyst shows H_2 desorption peaks at 70, 490 and 720 °C, while the Ni/LaAl catalyst at 40, 160, 480, 750 and 810 °C. As is well understood, H_2 desorption peaks at temperatures lower than 450 °C can be assigned to H_2 desorbed from the active metal sites, while peaks located at temperatures higher than 450 °C may come from H_2 located in the subsurface layers, H_2 spillover and/or reoxidation of Ni by water inherent on the sample after reduction.[54,55] Ni dispersion (D_{Ni}, %) and the mean Ni particle size (d_{Ni}, nm) of the catalysts were calculated based on the amount of H_2 desorbed (<450 °C), and the results are presented in Table 2.

The high resolution XPS Ni 2p spectra for the reduced Ni/Al and Ni/LaAl catalysts are presented in Fig. S3,† while the accompanying elemental compositions are given in Table 3. For the Ni $2p_{3/2}$ peak, both catalysts present a low binding energy shoulder corresponding to Ni^0 at around 853.0 eV and a strong peak at 856.1 ± 0.2 eV corresponding to $NiAl_2O_4$.[56] The presence of $NiAl_2O_4$ is in agreement with the XRD results, where this is the only Ni oxide observed. From the O 1s spectra (not shown herein) the peak identified at binding energies 531.2 ± 0.1 eV corresponds to lattice oxygen for Al_2O_3. Also, it can be seen (Table 3) that in the presence of La, more Ni prefers to reside on the surface (higher Ni surface atomic concentration).

Fig. 5 shows representative transmission electron microscopy images with different magnifications and the mean Ni particle size distribution histograms for the reduced Ni/Al and
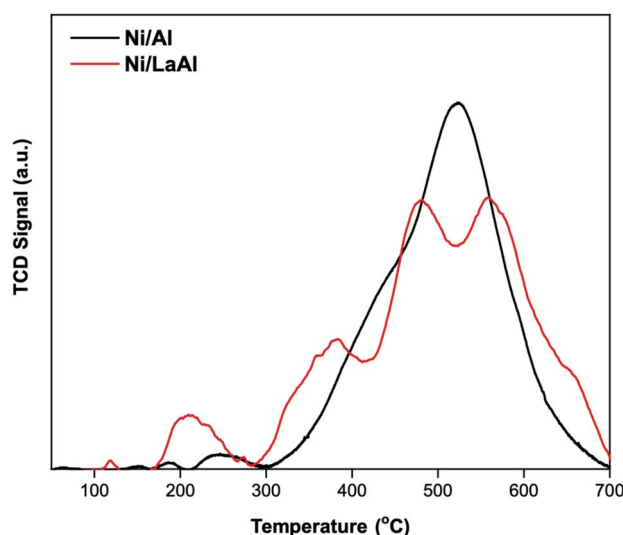

Fig. 4 H_2-TPR profiles obtained over the Ni/Al and Ni/LaAl catalysts.

Table 2 Ni dispersion and mean particle size

Catalyst	D_{Ni}, %	d_{Ni}, nm	$d_{(Ni)}^a$, nm
Ni/Al	6.0	16.1	4.3
Ni/LaAl	12.6	7.7	6.0

[a] Based on TEM imaging.

© 2021 The Author(s). Published by the Royal Society of Chemistry

Table 3 XPS determined surface elemental concentrations and core level peak maxima for the Ni/Al and Ni/LaAl reduced catalysts

Catalyst	Element	O (1s)	Al (2p)	La (2p)	Ni (2p)
Ni/Al	Element. conc. (at%)	63.48	34.31		2.21
Ni/LaAl	Binding energy (eV)	531.24	74.27		856.31
Ni/Al	Element. conc. (at%)	62.08	33.62	0.45	3.85
Ni/LaAl	Binding energy (eV)	531.19	74.21	836.22	856.16

Ni/LaAl catalysts. It appears that for both catalysts the distribution of Ni particles on the support is quite uniform and rather homogeneously deposited on the surface. As a result of the relatively low calcination/reduction temperatures used herein (400 °C), the average Ni size (Fig. 5d and h) was rather small, estimated at 4.3 ± 1.6 nm for the Ni/Al and 6.0 ± 1.6 nm for the Ni/LaAl.

3.2 Catalytic activity

3.2.1 Effect of hydrotreating temperature. The SDO of palm oil over the Ni/Al and Ni/LaAl catalysts was carried out between 300–400 °C and for comparison purposes, the H_2 pressure, LHSV and H_2/oil feed ratio were kept constant at 30 bar, 1.2 h^{-1} and 1000 cm^3 (cm^3)$^{-1}$, respectively. It is clarified that the results presented herein are those obtained at the end of the short time-on-stream experiments, *i.e.*, after 6 h (experimental protocol #1). It is noted that both catalysts exhibited very stable values during these 6 h, without any discernible loss in activity (Fig. S4†). The reproducibility of the experimental results was tested by carrying out a number of repeat experiments (at least

three times). From these experiments, 95% confidence intervals for the mean value were calculated and, as can be seen in Fig. S5,† the individual experimental values lay well within the corresponding confidence intervals showing a very good reproducibility of the repeated experiments. Moreover, for both catalysts, the analysis of the liquid products showed the production of only n-C_8–C_{18} hydrocarbons and of the gaseous products, the presence of H_2, CO, CO_2, CH_4, C_2H_6 and C_3H_8; however, as the latter two gases were in trace amounts, they were not quantified.

As is well understood, it is important to ensure operation at steady state conditions in order to accurately evaluate catalytic performance. The group of Crocker *et al.*[57,58] reported two highly interesting works devoted to the transformation of used cooking oil and waste free fatty acids into green diesel *via* decarboxylation/decarbonylation (deCO$_x$) reactions using Ni based catalysts. In contrast to our study, they found that the prepared catalytic materials required >24 or even 48 h of time-on-stream in order to attain steady state conditions. However, the period of time required in order to attain steady state conditions in the system is highly dependent on both the catalyst and the reaction conditions employed. Similar behavior to our study was observed by Veses *et al.*[59] and Alvarez-Galvan *et al.*,[60] who reported that steady state was achieved after 45 min and 2–3 h, respectively.

The hydrotreating temperature has an important effect on the SDO reaction, as it affects the extent that decarboxylation/decarbonylation, hydrodeoxygenation, isomerization and hydrocracking reactions occur and the catalyst's lifetime.[61–63] As an example, Srifa *et al.*,[61] using palm oil as feedstock over a NiMoS$_2$/γ-
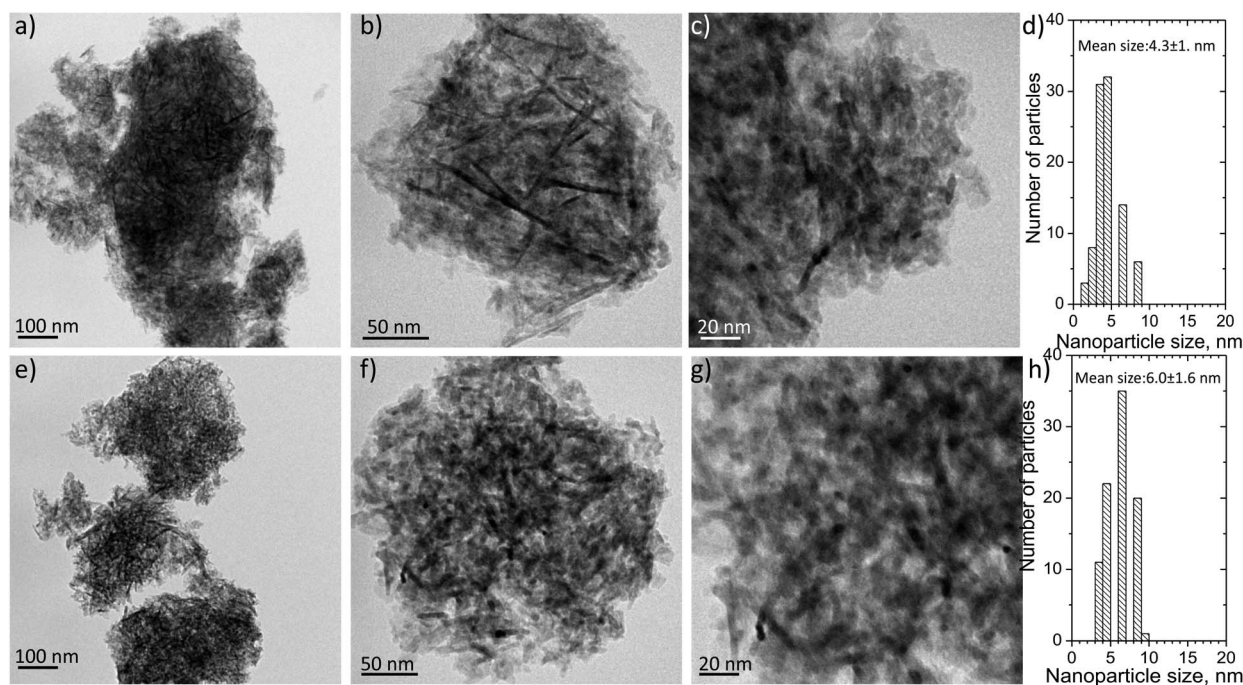

Fig. 5 (a–c) TEM images of the reduced Ni/Al catalyst at different magnifications, (d) Histogram showing the particle size distributions of n X NPs (data obtained from TEM image analysis), (e–g) TEM images of reduced Ni/LaAl catalyst at different magnifications, and (h) Histogram showing the particle size distributions of n X NPs (data obtained from TEM image analysis).

Al_2O_3 catalyst, reported that a small increase in the reaction temperature (from 270 to 300 °C) resulted at considerable improvement in the selectivity towards C_{15}–C_{18} hydrocarbons (from 26.7% to 89.8%). Moreover, Šimáček et al.[63] using a commercial hydrorefining Ni–Mo/γ-Al_2O_3 catalyst in the hydrodeoxygenation of rapeseed oil, reported that the liquid products obtained below 310 °C contained reactants and intermediates, while over 310 °C the liquid products contained only C_{17} and C_{18} hydrocarbons.

For comparison purposes, a blank experiment at 375 °C (experimental protocol #1) was performed in order to determine the liquid product distribution during palm oil deoxygenation in the absence of catalyst. The results showed that the liquid products were mainly composed of fatty acids (>76%) with low hydrocarbon yield (<24%) (Table S1†). Thus, it can be concluded that the thermal contributions to the production of diesel-like hydrocarbons are relatively minor.

The influence of hydrotreating temperature on the triglyceride conversion for the Ni/Al and Ni/LaAl catalysts tested herein is presented in Fig. 6a, and as can be observed, conversion increased with increasing temperature for both catalysts. However, the Ni/LaAl catalyst appears more active at low

reaction temperatures, with conversion taking the value of 85% at 300 °C (54% for the Ni/Al) and 87% at 325 °C (79% for the Ni/Al). Above 350 °C, both catalysts showed similar conversion, which reached 100% at 375 °C, and declined slightly at 400 °C. In broad agreement with our results, Ramesh et al.,[64] examining the performance of Ni–MoS/mesoporous zirconia–silica (Zr-SBA-15, Zr-KIT-6, Zr–SiO_2, and Zr-FSM-16 with Si/Zr = 10) catalysts on the hydrodeoxygenation of jojoba oil between 225–375 °C (at a constant H_2 pressure of 30 bar), reported a slight decrease in the conversion of triglycerides, when the temperature increased over 350 °C.

The influence of hydrotreating temperature on the n-C_8 to n-C_{18} hydrocarbon yield is presented in Fig. 6b. As can be observed, the yield to n-C_{15} to n-C_{18} hydrocarbons increased between 300–375 °C, for both catalysts, and the values attained for the Ni/LaAl (in parenthesis the corresponding one for the Ni/Al) were: 78% (38%) at 300 °C, 80% (62%) at 325 °C, 82% (75%) at 350 °C and 89% (90%) at 375 °C; however, it decreased to 78% (84%) at 400 °C. It is speculated that the slight decrease in the conversion of triglycerides (Fig. 6a) and n-C_{15} to n-C_{18} hydrocarbons at 400 °C (Fig. 6b) was caused by the sintering of the
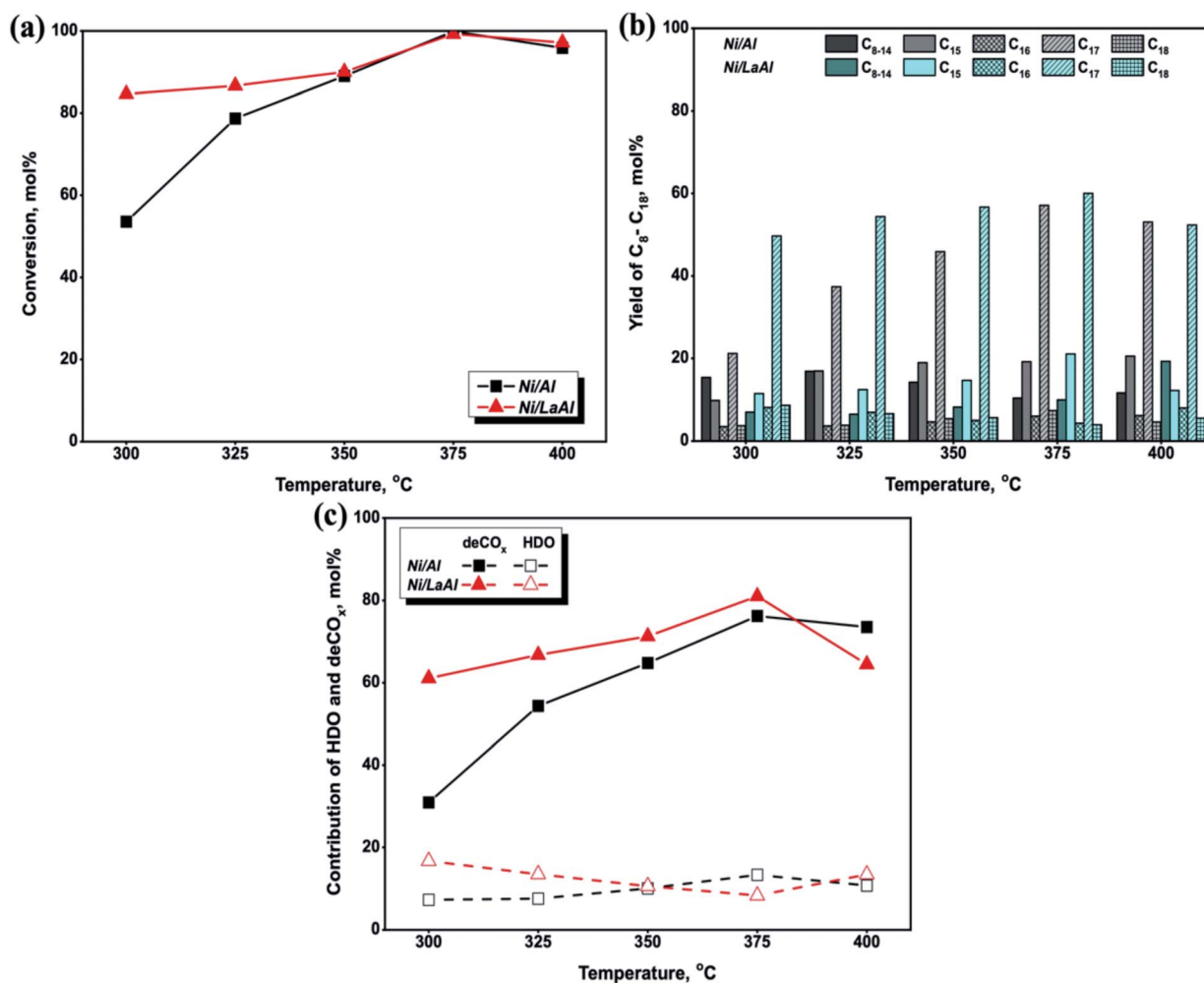

Fig. 6 Effect of temperature on: (a) palm oil conversion, (b) paraffin yield, and (c) % contribution of HDO and deCO$_x$, for the Ni/Al and Ni/LaAl catalysts. Reaction conditions: T = 300–400 °C, P = 30 bar, LHSV = 1.2 h^{-1}, H_2/oil = 1000 cm^3 $(cm^3)^{-1}$.

active phase and the formation of coke on the catalysts surface. This finding is in accordance with the literature,[64–66] where it has been argued that the optimum reaction temperature for the C=O bond scission of free fatty acids, with minimum degree of carbon deposition during the SDO process, is in the range of 350–375 °C; a further increase of temperature to 400 °C and above leads to coke formation due to the occurrence of cracking/hydrocracking reactions, the complex oil composition and the large molecules.

Furthermore, as illustrated in Fig. 6b, the n-C_{17} and n-C_{15} hydrocarbons were always higher for both catalytic samples, which indicates a promotion of the $deCO_2$ and deCO reaction pathways. Specifically, for the Ni/Al catalyst, the yield of n-C_{17} gradually increased from 21% at 300 °C to the maximum value of 57% at 375 °C, while the yield of n-C_{15} also increased from 10% to 19%. However, the Ni/LaAl catalyst showed higher n-C_{17} and n-C_{15} yields, with values for the former hydrocarbon ranging from 49 to 60% and for the latter from 11 to 21%, between 300 and 375 °C. Moreover, although the yield of n-C_{18} and n-C_{16} hydrocarbons was less than 10% (between 300–375 °C) for both catalysts, an opposing trend was observed, $i.e.$, it increased for the Ni/Al and decreased for the Ni/LaAl sample. Specifically, for the former catalyst, the yield of n-C_{18} increased from 4% 7% and the yield of n-C_{16} rose from 4% to 6%, from 300 °C to 375 °C respectively. In contrast, the n-C_{18} and n-C_{16} yield for the Ni/LaAl catalyst declined between 300–375 °C, taking values from 9% to 4% and from 8% to 4%, respectively.

Another difference between the catalysts tested was observed in terms of the yield towards lighter n-C_8–C_{14} hydrocarbons. Specifically, for the Ni/Al catalyst the yield of n-C_8–C_{14} decreased from 15% to 10%, which may be explained by secondary catalytic cracking of the intermediates produced. Chen et $al.$,[67] studied the catalytic performance of 10 wt% Ni/HZSM-5 (Si/Al = 25) catalyst on the hydroprocessing of fatty acid methyl esters (FAME) at temperatures between 260 °C and 300 °C and at H_2 pressures ranging from 4–12 bar and reported that when increasing the reaction temperature from 260 °C to 300 °C, under any level of H_2 pressure (4, 8 and 12 bar), the yield of C_8–C_{16} hydrocarbons decreased, and attributed this finding to secondary catalytic cracking of the intermediates produced. In contrast with the Ni/Al catalyst, the yield of n-C_8–C_{14} for the Ni/LaAl increased from 7% to 10% from 300 to 375 °C (and to 19% at 400 °C), indicating that at higher hydrotreating temperatures, cracking occurs along with the $deCO_x$ reactions, leading to the formation of hydrocarbons with lower molecular weight.[16,63,68]

The results reported above are in full agreement with those obtained by the groups of Srifa et $al.$[69] and Liu et $al.$[70] In particular, Srifa et $al.$[69] studied the hydrodeoxygenation of palm oil over $NiAl_2O_4$ spinel-type catalysts, with different reduction temperatures at 330 °C, 50 bar, LHSV of 1 h^{-1} and H_2/oil feed ratio of 1000 N cm^3 (cm^3)$^{-1}$ and reported that the $deCO_x$ reactions were dominant over the HDO pathway. Liu et $al.$[70] studied the transformation of jatropha oil into green diesel in a fixed bed reactor over five catalytic materials supported on γ-Al_2O_3 as follows: $5Ni_{15}Mo/Al_2O_3$ catalyst in both sulfided and non-sulfided state and $5Ni_{15}Mo_{0.5}La/Al_2O_3$, $5Ni_{15}Mo_5La/Al_2O_3$, $5Ni_{15}Mo_{15}La/Al_2O_3$ non-sulfided catalysts. The catalytic tests

were carried out at 280–400 °C, 35 bar, LHSV of 0.9 h^{-1} and H_2/oil feed ratio of 1000 cm^3 (cm^3)$^{-1}$. The authors reported that the highest C_{15}–C_{18} hydrocarbons yield was achieved by the $5Ni15Mo5La/Al_2O_3$ non-sulfided catalyst at 370 °C taking value equal to 78%. Moreover, the C_{15}–C_{18} fraction greatly increased from 280 °C to 370 °C, however, between 370 °C to 400 °C there was no significant effect on the C_{15}–C_{18} yield. Furthermore, the light fraction yield increased with temperature, as higher temperatures favored the cracking reaction.

In order to clarify further the deoxygenation behavior of the catalysts tested herein, the mol% contributions of HDO and deCO/$deCO_2$ reactions were calculated using eqn (6) and (7) and the results are presented in Fig. 6c. The results confirm that both the Ni/Al and Ni/LaAl catalysts promoted the $deCO_2$ and deCO deoxygenation paths much more extensively than HDO, for the entire temperature range under investigation. These results are consistent with published works reporting that Ni based catalysts favor the $deCO_x$ reaction paths and not the HDO reaction.[9,41,69,71] Moreover, as the palm oil used in the present study consisted mainly of C_{16} and C_{18} fatty acids, it can be deduced that the main components of the liquid products should be n-C_{15} and n-C_{17} hydrocarbons due to the highly selective $deCO_x$ reaction paths.

As mentioned above, the main gaseous products were H_2, CO_2, CO and CH_4 and the results are presented in Table 4. Leaving aside H_2, which was used as feed, CH_4 was the main gas product due to the methanation reaction between CO or CO_2 with H_2. The presence of C_2H_6 and C_3H_8 in only trace amounts indicates their cracking, producing CH_4. An interesting observation is that CO_2 seems to be produced in slightly higher amounts than CO, which may possibly indicate that CO is relatively easier to hydrogenate to CH_4.[72] The above are in line with the findings reported by a number of published works concerning the influence of Ni catalysts on the selectivity of the gaseous products.[9,41,65,73,74]

In concluding, the improved catalytic activity exhibited by the Ni/LaAl catalyst can be probably understood on the basis of the increased dispersion of Ni on its surface (XPS) and the increased Ni–support interaction (H_2-TPR). Moreover, it is likely

Table 4 Effect of hydrotreating temperature on gas product composition for the Ni/Al and Ni/LaAl catalysts during SDO of palm oil. Reaction conditions: T = 300–400 °C, P = 30 bar, LHSV = 1.2 h^{-1}, H_2/oil = 1000 cm^3 (cm^3)$^{-1}$

Catalysts	Temperature (°C)	Gas product composition (mol%)			
		CO_2	H_2	CH_4	CO
Ni/Al	300	2.80	90.64	6.22	0.36
	325	2.03	91.59	6.38	0.00
	350	4.04	86.30	7.97	1.68
	375	2.92	91.82	4.66	0.60
	400	2.21	88.67	9.11	0.00
Ni/LaAl	300	3.32	87.07	9.16	0.45
	325	3.39	88.56	7.34	0.71
	350	2.69	89.89	6.70	0.72
	375	2.82	86.73	10.45	0.00
	400	2.19	79.77	16.93	1.11

that the lower overall acidity of the Ni/LaAl catalyst (TPD) suppressed the hydrocracking reactions, which helps explain its improved yield towards C_{15}–C_{18} alkanes.

3.2.2 Effect of LHSV. The effect of LHSV (Fig. 7) was examined in the range of 1.2–3.6 h^{-1} at the optimum temperature identified above, *i.e.*, at 375 °C ($P = 30$ bar and H_2/oil = 1000 cm^3 $(cm^3)^{-1}$). As can be observed, an increase of the LHSV reduced both the conversion of the triglycerides (Fig. 7a) and the yield towards n-C_{15}–C_{18} paraffins (Fig. 7b), a result of the decreased contact time between the feed and the catalyst. Specifically, for the Ni/Al conversion decreased from 100% at 1.2 h^{-1} to 67% at 2.4 h^{-1} and 57% at 3.6 h^{-1} and although this decrease was smaller for the Ni/LaAl catalyst, it was still significant (the corresponding values were: 100%, 83% and 65%). Similarly, the yield to n-C_{15} to n-C_{18} paraffins decreased for the Ni/Al from 90%, to 52%, to 44% and for the Ni/LaAl from 90%, to 71%, to 53% at LHSV of 1.2, 2.4 and 3.6 h^{-1}, respectively. However, this decrease was mainly caused by a substantial decrease in the yield of n-C_{17}, which for the Ni/Al catalyst dropped from 57% to 22% and for the Ni/LaAl from 60% to 29%, at 1.2 h^{-1} and 3.6 h^{-1}, respectively. Another observation

was that the increase in the LHSV resulted at a marginal increase in the yield to n-C_8–C_{14} hydrocarbons for both catalysts (from 10 to 13% for the Ni/Al and from 10 to 12% for the Ni/LaAl). Thus, as illustrated in Fig. 7c, the contribution of the deCO$_x$ reactions decreased with increasing the LHSV, taking the values, for the Ni/Al catalyst, of 76% (1.2 h^{-1}), 43% (2.4 h^{-1}) and 36% (3.6 h^{-1}). For the Ni/LaAl, the corresponding values stood at 81%, 59% and 46%. The analysis of the composition of the gas products (Table 5) showed that methane was the major gas product produced from the hydrogenation of CO_2 and CO.

Similar results with the ones reported herein were obtained by Kaewmeesri *et al.*[41] and Nimkarde *et al.*[75] In particular, Kaewmeesri *et al.*[41] observed that the maximum C_{15}–C_{18} product yield (82%) was achieved for the lowest LHSV (0.5 h^{-1}), as there was sufficient contact time between the reactant and the catalyst, while increasing the LHSV to 2 h^{-1} caused a decrease to 66%. Moreover, the authors also showed that deCO$_x$ was the dominant reaction pathway and that methane was the main gas product generated from CO_2/CO hydrogenation. Nimkarde *et al.*[75] investigated the effect of LHSV (1.1–4.5 h^{-1}) during the hydrodeoxygenation of karanja oil and showed
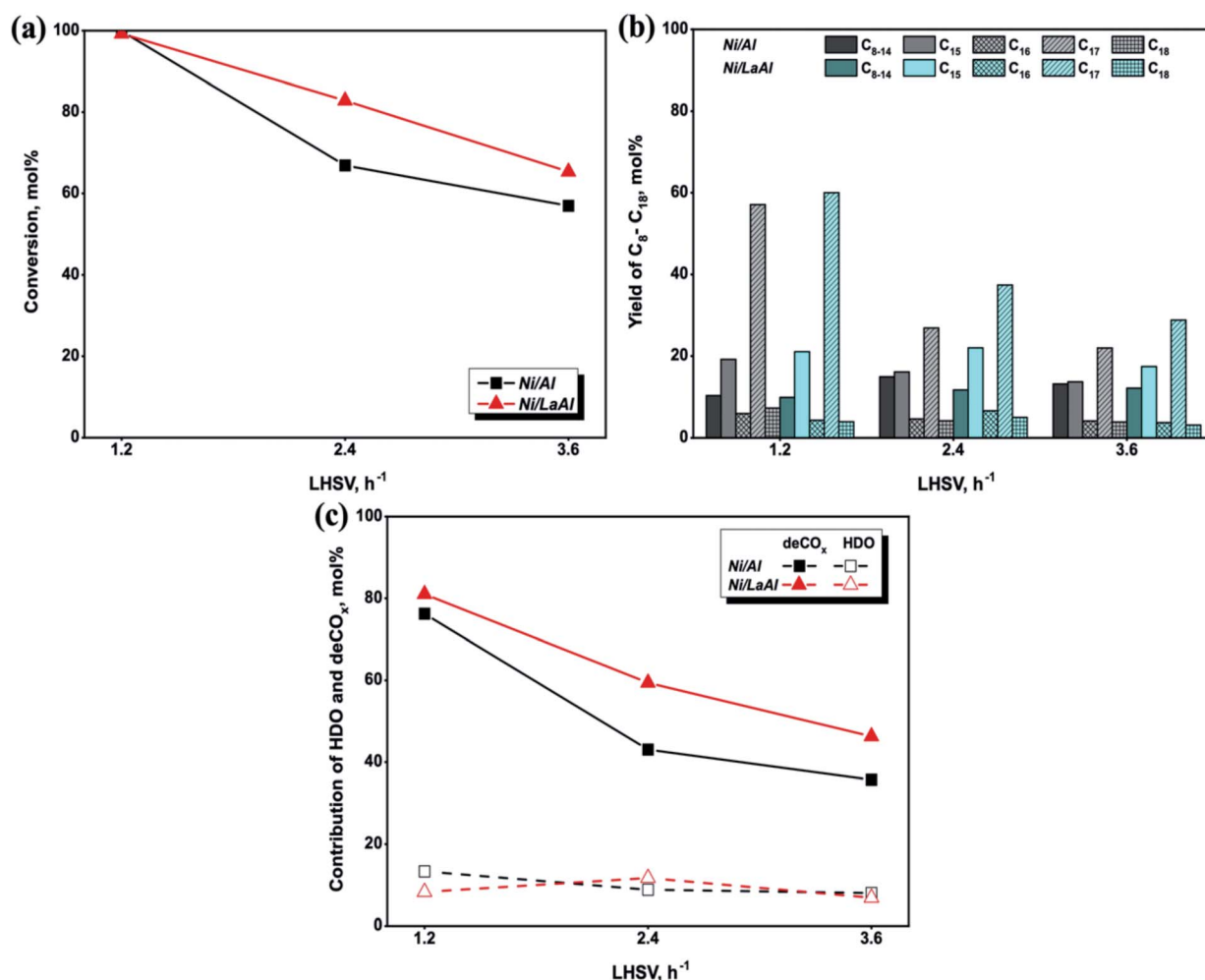

Fig. 7 Effect of LHSV on: (a) palm oil conversion, (b) paraffin yield, and (c) % contribution of HDO and deCO$_x$, for the Ni/Al and Ni/LaAl catalysts. Reaction conditions: $T = 375$ °C, $P = 30$ bar, LHSV = 1.2–3.6 h^{-1}, H_2/oil = 1000 cm^3 $(cm^3)^{-1}$.

Table 5 Effect of LHSV on gas product composition for the Ni/Al and Ni/LaAl catalysts during SDO of palm oil. Reaction conditions: $T = 375\ ^\circ C$, $P = 30$ bar, LHSV = 1.2–3.6 h^{-1}, H_2/oil = 1000 cm^3 $(cm^3)^{-1}$

Catalysts	LHSV (h^{-1})	Gas product composition (mol%)			
		CO_2	H_2	CH_4	CO
Ni/Al	1.2	2.92	91.82	4.66	0.60
	2.4	2.21	92.86	4.39	0.53
	3.6	2.87	91.69	4.86	0.58
Ni/LaAl	1.2	2.82	86.73	10.45	0.00
	2.4	19.06	51.30	25.42	4.22
	3.6	18.37	67.93	13.69	0.00

that at 380 °C, conversion decreased from 88.6% (1.1 h^{-1}) to 58.3% (4.5 h^{-1}) and from 90.5% (1.1 h^{-1}) to 61% (4.5 h^{-1}) over CoMo and NiMo catalysts, respectively.

3.3 Catalyst stability and carbon deposition studies

3.3.1 Catalyst stability. The stability of the catalysts tested herein was investigated through 20 h time-on-stream experiments that were carried out at $T = 375\ ^\circ C$, $P = 30$ bar, LHSV = 1.2 h^{-1} and H_2/oil feed ratio = 1000, *i.e.*, the optimum experimental conditions, as identified above. The results obtained are presented in Fig. 8, and as can be observed, triglyceride conversion decreased substantially for the Ni/Al catalyst, dropping from an initial value of 92% to 50% at the end of the experiment. Similarly, the yield towards n-C_{15} decreased from 18% to 6% and for n-C_{17} from 51% to 28%. In contrast, the Ni/LaAl catalyst exhibited a considerably more stable performance, as conversion decreased from 98% to 86%, the yield towards n-C_{15} from 12% to 8% and for n-C_{17} from 58% to 49%, after 20 h of time-on-stream. Another interesting observation is that the yield to n-C_{16} and n-C_{18} decreased for the Ni/Al catalyst (from 8% to 5% and from 7% to 3%, respectively), while it increased for the Ni/LaAl catalyst (from 4% to 5% and from 3% to 6%, respectively). The deactivation experienced by the Ni/Al and Ni/LaAl catalysts may be related to the adsorption of unsaturated

Fig. 8 Palm oil conversion and paraffin yield for the Ni/Al and Ni/LaAl catalysts during 20 h time-on-stream experiments. Reaction conditions: $T = 375\ ^\circ C$, $P = 30$ bar, LHSV = 1.2–3.6 h^{-1}, H_2/oil = 1000 cm^3 $(cm^3)^{-1}$.

triglycerides on their surface, which would lead to coke formation on the acidic sites, and/or to the sintering of the nickel species;[33] the effect of these issues on the performance of each catalyst is addressed in the following section.

Taromi *et al.*,[33] using canola oil as feed and similar experimental conditions to the ones reported herein (*i.e.*, $T = 400\ ^\circ C$, $P = 35$ bar, H_2/oil = 600 cm^3 $(cm^3)^{-1}$, LHSV = 0.5 h^{-1}), also observed substantial deactivation for Ni/Al_2O_3 catalysts. Specifically, after a rather stable operation for approximately 5 h, the conversion values recorded for a Ni/Al_2O_3 catalyst, prepared *via* incipient wetness impregnation, decreased from about 80% to 35% after 10 h. Interestingly, a Ni/Al_2O_3 catalyst prepared *via* sol gel was more stable as conversion declined from 69% to 54% after 10 h of operation. Lercher *et al.*,[44] using algal oil as feed, reported that a Ni/ZrO_2 catalyst did not deactivate after 72 h of time-on-stream tests however, the experiments were conducted at a lower temperature (260 °C) and with a more dilute feed (1.33 wt%, LHSV = 0.32 h^{-1}) thus, the conditions were milder in comparison to those reported herein.

3.3.2 Carbon analysis and further characterization of spent catalysts. As it is well understood, the deactivation of Ni based catalysts during the conversion of hydrocarbons at elevated temperatures is due to two main reasons, *i.e.*, the deposition of carbon on their surface and metal particle sintering. Sintering is the process where the metallic particles that constitute the active phase grow in size during the reaction and it may occur either through the migration of entire particles over the support and their coalescence with other particles located nearby or through the migration of atoms over the support from one crystallite to a neighboring crystallite (Ostwald ripening).[76,77] In effect, sintering not only reduces the number of active sites available to the reactants, but can also induce carbon deposition during the reaction, as larger metallic particles stimulate the formation of coke. Carbon deposition is the result of the elevated temperatures that are necessary in order to raise the molecular energy for the cleavage of the C–H and C–O bonds of the reactants.[78,79] In order to investigate the extent that these two phenomena occurred, and their effect on catalytic stability, the spent catalysts derived after the long term time-on-stream experiments (experimental protocol #2) were investigated using TGA, TPO, Raman and TEM.

Fig. 9a presents the TGA results for both catalysts. This initial examination revealed that the amount of coke deposited on the Ni/LaAl catalyst was significantly lower (11%) than that deposited on the Ni/Al catalyst (17%). Further examination of the two spent catalysts was carried out using temperature programmed oxidation (TPO, Fig. 9b). It is generally accepted in the literature that, in air rich environments, functional groups physically or chemically adsorbed onto carbon nanomaterials decompose below 200 °C, amorphous carbon species combust at temperatures between 200–500 °C, carbon nanofibers (CNFs) and carbon nanotubes (CNTs) are burned between 500–600/650 °C, and more graphitic structures such as graphite and graphene combust between 600/650–800 °C.[80,81] For the Ni/Al catalyst, the peak around 210 °C can likely be ascribed to atomic carbon deposits formed over metallic nickel (which is the most reactive carbon type to oxygen), while the shoulder
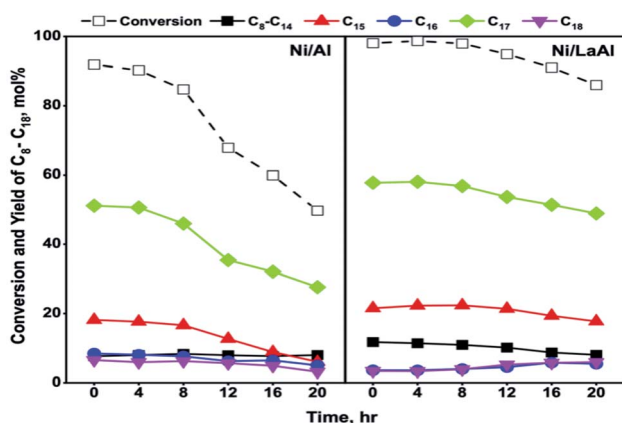
around 475 °C can be attributed to amorphous coke deposited close to the metal support interphase.[82] The largest oxidation peak, at around 635 °C, can be linked to well defined-structured carbon, hard to be oxidized. For the Ni/LaAl catalyst, atomic carbon appears as a shoulder (at around 240 °C) of the peak located at 335 °C. The graphitic carbon peak at 630 °C is significantly less pronounced in comparison to the Ni/Al. Two additional thermal processes should also be taken into consideration; decomposition of the La(OH)$_3$ and LaO$_2$CO$_3$ phases that take place at around 350 °C and 750 °C, respectively, as carbonates are more stable than the hydroxides.[83]

The nature and structure of the carbonaceous species deposited on to the spent catalysts was also investigated using Raman spectroscopy and as can be observed in Fig. 10a and b, both catalysts show two well resolved bands around 1340 cm^{-1} and 1580 cm^{-1}. The former (D band) results from a disorder-double resonant process due to breakdown of the usual wave vector selection rule (A$_{1g}$ symmetry), while the latter (G-band), located at the centre of the Brillouin zone (BZ), is caused by the in-plane optical mode of vibration (E$_{2g}$ symmetry) of two neighboring carbon atoms on the perfect hexagonal

graphite.[84,85] As it is widely accepted,[78,86] the relative intensity of the D and G bands (I_D/I_G) can be used to describe the structural order of carbon deposits with lower values indicating a higher degree of graphitization. The I_D/I_G values obtained for the catalysts tested herein where 0.85 for the Ni/Al and 0.91 for the Ni/LaAl, meaning that although the degree of graphitization was not very high for both catalysts, higher fractions of difficult to oxidize structures were deposited on the Ni/Al catalyst, in excellent agreement with the TPO results presented above. Deconvolution of the Ni/Al pattern shows the presence of four peaks, namely, D1 ($\sim$1233 cm^{-1}), D2 ($\sim$1329 cm^{-1}), D3 (1430 cm^{-1}) and G (1582 cm^{-1}). On the other hand, in the case of Ni/LaAl catalyst the deconvoluted Raman peaks were D1 (1228 cm^{-1}), D2 (1329 cm^{-1}), D3 (1397 cm^{-1}) and G1 (1580 cm^{-1}), G2 (1603 cm^{-1}). The origin of the peaks has as follows: G band is linked to graphitic planes, whereas D1 is a sp^2-sp^3 carbon structure, D2 band is associated to functional groups and disturbances caused by them in the graphene layer. The D3 band is linked to the presence of amorphous carbon (soot).[87]

Finally, the morphology of the carbonaceous deposits was probed using TEM (Fig. 11), which failed to identify any clear
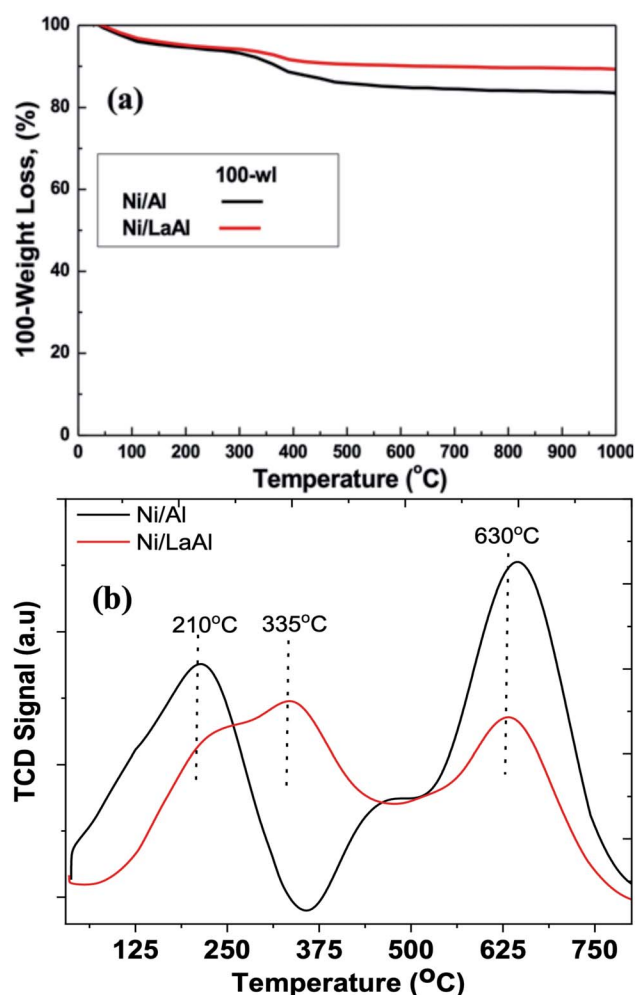

Fig. 9 (a) TGA graphs, and (b) TPO profiles of the spent Ni/Al and Ni/LaAl catalysts. Reaction conditions: experimental protocol #2.
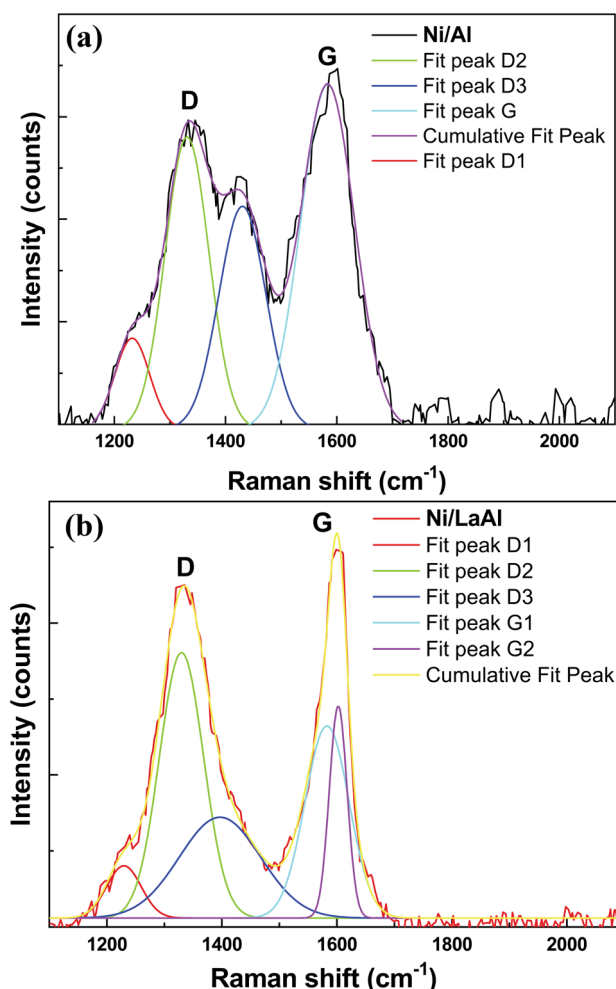

Fig. 10 Raman spectra of the spent (a) Ni/Al, and (b) Ni/LaAl catalysts. Reaction conditions: experimental protocol #2.
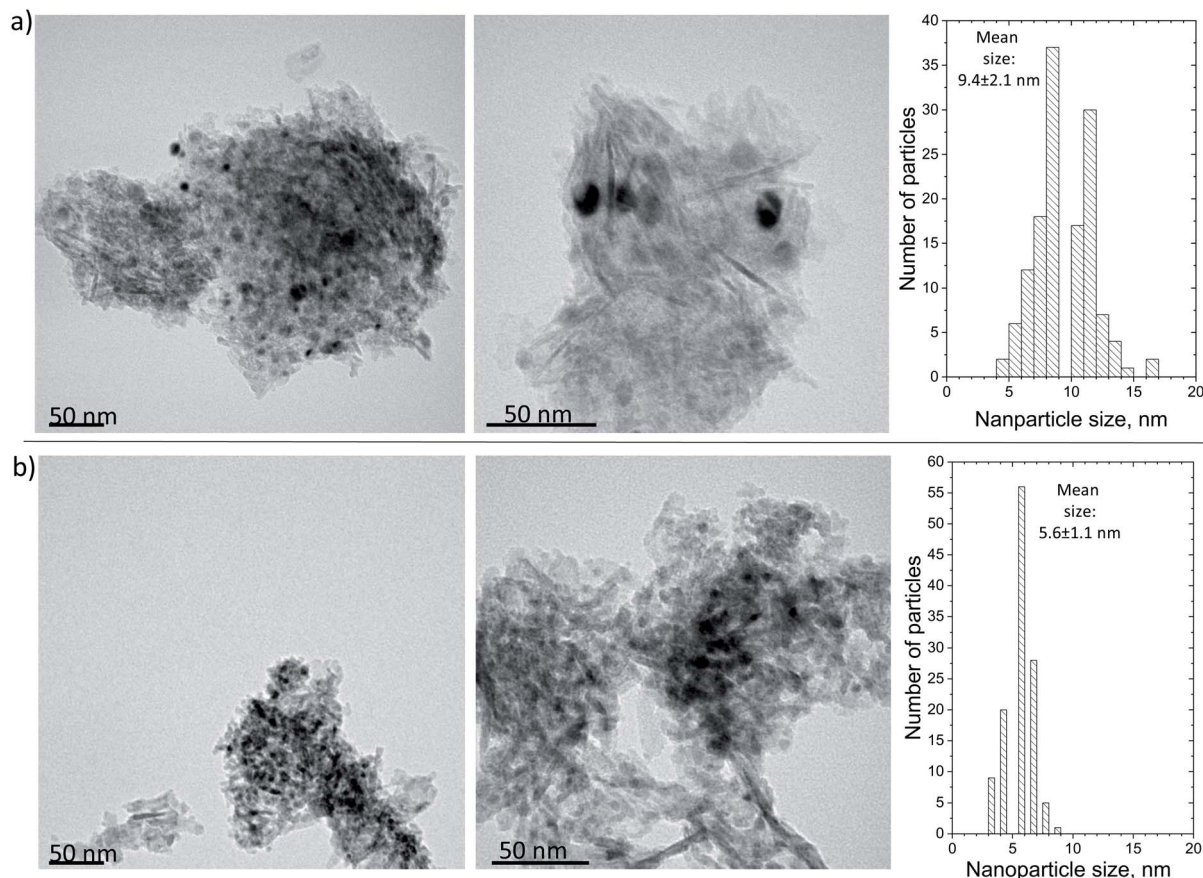
Fig. 11 TEM images and particle size distribution histogram of the spent: (a) Ni/Al, and (b) Ni/LaAl catalysts. Reaction conditions: experimental protocol #2.

carbon structures on either of the spent samples. This finding indicates that the surface coke formed a very thin layer not detectable at the working magnification and is in line with the TPO and Raman findings discussed above, *i.e.*, that the deposited carbon had a relatively low degree of graphitization. However, the calculation of the Ni mean nanoparticle size showed that while the Ni/Al suffered from extensive sintering (from 4.3 ± 1.6 nm for the reduced catalyst to 9.4 ± 2.1 nm for the spent), this was mostly avoided on the Ni/LaAl catalyst (from 6.0 ± 1.6 nm for the reduced catalyst to 5.6 ± 1.1 nm for the spent). This finding provides a good explanation for the excellent stability characteristics observed for this sample.

4 Conclusions

The present study investigated the effect of hydrotreating temperature and LHSV on the catalytic performance of Ni catalysts supported on γ-Al_2O_3 and γ-Al_2O_3 modified with La_2O_3, in a continuous flow trickle bed reactor, for the selective deoxygenation of palm oil. Catalytic experiments were performed between 300–400 °C, at a constant temperature (30 bar) and different LHSV (1.2–3.6 h^{-1}). The catalysts were prepared *via* the wet impregnation method, at a constant metal loading of 8 wt%. The catalytic samples, after calcination and/or reduction, were characterized by N_2 adsorption/desorption, XRD,

NH_3-TPD, CO_2-TPD, H_2-TPR, H_2-TPD, XPS and TEM, in order to provide an insight into the effect on performance by the their physical and chemical properties. Moreover, the spent catalysts after 20 h of time-on-stream tests were characterized by TGA, TPO, Raman and TEM, in order to determine the extent of carbon deposition and metal particle sintering on the spent samples.

The results show that the incorporation of La_2O_3 in the Al_2O_3 support: (i) increased the Ni surface atomic concentration (XPS), (ii) affected the nature and abundance of surface basicity as the concentration of basic sites was found to be 34.2 mmol CO_2 per g_{cat} for the Ni/Al and 47 mmol CO_2 per g_{cat} for the Ni/LaAl (the density of the basic sites was 0.216 and 0.33 mmol CO_2 per g_{cat}, respectively), and (iii) led to a drop in surface acidity from 200 mmol g_{cat}^{-1} (Ni/Al) to 170 mmol g_{cat}^{-1} (Ni/LaAl) and to the density of the acid sites from 1.26 mmol NH_3 per m^2 (Ni/Al) to 1.19 mmol NH_3 per m^2 (Ni/LaAl); however, the Ni/LaAl catalyst presented a larger population of medium-strength acid sites. These characteristics helped promote the SDO process and prevented extended cracking and the formation of coke. Thus, higher triglyceride conversions and n-C_{15} to n-C_{18} hydrocarbon yields were achieved with the Ni/LaAl at lower reaction temperatures. Moreover, the Ni/LaAl catalyst was considerably more stable during 20 h of time-on-stream. Examination of the spent catalysts revealed that both carbon deposition and degree of graphitization of the surface coke, as

well as, the extent of sintering were lower on the Ni/LaAl catalyst, explaining its excellent performance during time-on-stream.

Conflicts of interest

There are no conflicts of interest to declare.

Acknowledgements

References

1 J. Zalasiewicz, C. N. Waters, C. P. Summerhayes, A. P. Wolfe, A. D. Barnosky, A. Cearreta, P. Crutzen, E. Ellis, I. J. Fairchild, A. Gałuszka, P. Haff, I. Hajdas, M. J. Head, J. A. Ivar do Sul, C. Jeandel, R. Leinfelder, J. R. McNeill, C. Neal, E. Odada, N. Oreskes, W. Steffen, J. Syvitski, D. Vidas, M. Wagreich and M. Williams, *Anthropocene*, 2017, **19**, 55–60.
2 X. Zheng, D. Streimikiene, T. Balezentis, A. Mardani, F. Cavallaro and H. Liao, *J. Cleaner Prod.*, 2019, **234**, 1113–1133.
3 P. Bareschino, E. Mancusi, M. Urciuolo, A. Paulillo, R. Chirone and F. Pepe, *Renewable Sustainable Energy Rev.*, 2020, **130**, 109962.
4 S. Liu, Q. Zhu, Q. Guan, L. He and W. Li, *Bioresour. Technol.*, 2015, **183**, 93–100.
5 S. L. Douvartzides, N. D. Charisiou, K. N. Papageridis and M. A. Goula, *Energies*, 2019, **12**, 809.
6 N. D. Charisiou, K. Polychronopoulou, A. Asif and M. A. Goula, *Surf. Coat. Technol.*, 2018, **352**, 92–111.
7 N. Vivek, R. Sindhu, A. Madhavan, A. J. Anju, E. Castro, V. Faraco, A. Pandey and P. Binod, *Bioresour. Technol.*, 2017, **239**, 507–517.
8 A. Afshar Taromi and S. Kaliaguine, *Fuel Process. Technol.*, 2018, **171**, 20–30.
9 A. Srifa, K. Faungnawakij, V. Itthibenchapong and S. Assabumrungrat, *Chem. Eng. J.*, 2015, **278**, 249–258.
10 R. W. Gosselink, S. A. Hollak, S. W. Chang, J. Van Haveren, K. P. De Jong, J. H. Bitter and D. S. Van Es, *ChemSusChem*, 2013, **6**, 1576–1594.
11 M. Grilc, B. Likozar and J. Levec, *ChemCatChem*, 2016, **8**, 180–191.
12 A. E. Coumans and E. J. Hensen, *Catal. Today*, 2017, **298**, 181–189.
13 E. Santillan-Jimenez, T. Morgan, R. Loe and M. Crocker, *Catal. Today*, 2015, **258**, 284–293.
14 E. Santillan-Jimenez, R. Loe, M. Garrett, T. Morgan and M. Crocker, *Catal. Today*, 2018, **302**, 261–271.
15 N. Asikin-Mijan, H. V. Lee, J. C. Juan, A. R. Noorsaadah, H. C. Ong, S. M. Razali and Y. H. Taufiq-Yap, *Appl. Catal., A*, 2018, **552**, 38–48.
16 C. Kordulis, K. Bourikas, M. Gousi, E. Kordouli and A. Lycourghiotis, *Appl. Catal., B*, 2016, **181**, 156–196.
17 J. A. Hunns, M. Arroyo, A. F. Lee, J. M. Escola, D. Serrano and K. Wilson, *Catal. Sci. Technol.*, 2016, **6**, 2560–2564.
18 H. Wang, H. Ruan, H. Pei, H. Wang, X. Chen, M. P. Tucker, J. R. Cort and B. Yang, *Green Chem.*, 2015, **17**, 5131–5135.
19 J. Wildschut, F. H. Mahfud, R. H. Venderbosch and H. J. Heeres, *Ind. Eng. Chem. Res.*, 2009, **48**, 10324–10334.
20 A. S. Berenblyum, R. S. Shamsiev, T. A. Podoplelova and V. Y. Danyushevsky, *Russ. J. Phys. Chem. A*, 2012, **86**, 1199–1203.
21 A. S. Berenblyum, T. A. Podoplelova, R. S. Shamsiev, E. A. Katsman and V. Y. Danyushevsky, *Pet. Chem.*, 2011, **51**, 336–341.
22 X. Zhu, L. L. Lobban, R. G. Mallinson and D. E. Resasco, *J. Catal.*, 2011, **281**, 21–29.
23 T. Nimmanwudipong, R. C. Runnebaum, D. E. Block and B. C. Gates, *Energy Fuels*, 2011, **25**, 3417–3427.
24 W. Jin, L. Pastor-Pérez, J. J. Villora-Pico, M. M. Pastor-Blas, A. Sepúlveda-Escribano, S. Gu, N. D. Charisiou, K. Papageridis, M. A. Goula and T. R. Reina, *Energies*, 2019, **13**, 132.
25 J. Chen and Q. Xu, *Catal. Sci. Technol.*, 2016, **6**, 7239–7251.
26 M. Rabaev, M. V. Landau, R. Vidruk-Nehemya, A. Goldbourt and M. Herskowitz, *J. Catal.*, 2015, **332**, 164–176.
27 B. Veriansyah, J. Y. Han, S. K. Kim, S. A. Hong, Y. J. Kim, J. S. Lim, Y. W. Shu, S. G. Oh and J. Kim, *Fuel*, 2012, **94**, 578–585.
28 T. Morgan, D. Grubb, E. Santillan-Jimenez and M. Crocker, *Top. Catal.*, 2010, **53**, 820–829.
29 K. N. Papageridis, G. Siakavelas, N. D. Charisiou, D. G. Avraam, L. Tzounis, K. Kousi and M. A. Goula, *Fuel Process. Technol.*, 2016, **152**, 156–175.
30 N. D. Charisiou, S. L. Douvartzides, G. I. Siakavelas, L. Tzounis, V. Sebastian, V. Stolojan, S. J. Hinder, M. A. Baker, K. Polychronopoulou and M. A. Goula, *Catalysts*, 2019, **9**, 676.
31 N. D. Charisiou, K. N. Papageridis, L. Tzounis, V. Sebastian, S. J. Hinder, M. A. Baker, M. AlKetbi, K. Polychronopoulou and M. A. Goula, *Int. J. Hydrogen Energy*, 2019, **44**, 256–273.
32 S. R. Yenumala, S. K. Maity and D. Shee, *Catal. Sci. Technol.*, 2016, **6**, 3156–3165.
33 A. Afshar Taromi and S. Kaliaguine, *Appl. Catal., A*, 2018, **558**, 140–149.
34 P. Kumar, S. R. Yenumala, S. K. Maity and D. Shee, *Appl. Catal., A*, 2014, **471**, 28–38.
35 I. Hachemi, N. Kumar, P. Mäki-Arvela, J. Roine, M. Peurla, J. Hemming, J. Salonen and D. Y. Murzin, *J. Catal.*, 2017, **347**, 205–221.
36 M. Gousi, C. Andriopoulou, K. Bourikas, S. Ladas, M. Sotiriou, C. Kordulis and A. Lycourghiotis, *Appl. Catal., A*, 2017, **536**, 45–56.

37 R. Loe, E. Santillan-Jimenez, T. Morgan, L. Sewell, Y. Ji, S. Jones, M. A. Isaacs, A. F. Lee and M. Crocker, *Appl. Catal., B*, 2016, **191**, 147–156.

38 N. D. Charisiou, G. Siakavelas, K. N. Papageridis, A. Baklavaridis, L. Tzounis, K. Polychronopoulou and M. A. Goula, *Int. J. Hydrogen Energy*, 2017, **42**, 13039–13060.

39 N. D. Charisiou, L. Tzounis, V. Sebastian, S. J. Hinder, M. A. Baker, K. Polychronopoulou and M. A. Goula, *Appl. Surf. Sci.*, 2019, **474**, 42–56.

40 A. Srifa, N. Viriya-Empikul, S. Assabumrungrat and K. Faungnawakij, *Catal. Sci. Technol.*, 2015, **5**, 3693–3705.

41 R. Kaewmeesri, A. Srifa, V. Itthibenchapong and K. Faungnawakij, *Energy Fuels*, 2015, **29**, 833–840.

42 K. N. Papageridis, N. D. Charisiou, S. L. Douvartzides, V. Sebastian, S. J. Hinder, M. A. Baker, S. AlKhoori, K. Polychronopoulou and M. A. Goula, *Fuel Process. Technol.*, 2020, **209**, 106547.

43 M. A. Goula, N. D. Charisiou, K. N. Papageridis, A. Delimitis, E. Pachatouridou and E. F. Iliopoulou, *Int. J. Hydrogen Energy*, 2015, **40**, 9183–9200.

44 B. Peng, X. Yuan, C. Zhao and J. A. Lercher, *J. Am. Chem. Soc.*, 2012, **134**, 9400–9405.

45 H. Ma, L. Zeng, H. Tian, D. Li, X. Wang, X. Li and J. Gong, *Appl. Catal., B*, 2016, **181**, 321–331.

46 N. D. Charisiou, G. Siakavelas, L. Tzounis, B. Dou, V. Sebastian, S. J. Hinder, M. A. Baker, K. Polychronopoulou and M. A. Goula, *Int. J. Hydrogen Energy*, 2020, **45**, 10442–10460.

47 W. Mo, F. Ma, Y. Ma and X. Fan, *Int. J. Hydrogen Energy*, 2019, **44**, 24510–24524.

48 D. Wierzbicki, R. Debek, M. Motak, T. Grzybek, M. E. Gálvez and P. Da Costa, *Catal. Commun.*, 2016, **83**, 5–8.

49 X. Li, H. Cheng, G. Liang, L. He, W. Lin, Y. Yu and F. Zhao, *Catalysts*, 2015, **5**, 759–773.

50 Y. X. Pan, C. J. Liu and P. Shi, *J. Power Sources*, 2008, **176**, 46–53.

51 K. Polychronopoulou, N. Charisiou, K. Papageridis, V. Sebastian, S. Hinder, A. Dabbawala, A. Alkhoori, M. Baker and M. Goula, *Nanomaterials*, 2018, **8**, 931.

52 Y. Kathiraser, W. Thitsartarn, K. Sutthiumporn and S. Kawi, *J. Phys. Chem. C*, 2013, **117**, 8120–8130.

53 N. D. Charisiou, A. Iordanidis, K. Polychronopoulou, I. V. Yentekakis and M. A. Goula, *Mater. Today: Proc.*, 2018, 27607–27616.

54 S. Ewald, S. Standl and O. Hinrichsen, *Appl. Catal., A*, 2018, **549**, 93–101.

55 S. Smeds, T. Salmi, L. P. Lindfors and O. Krause, *Appl. Catal., A*, 1996, **144**, 177–194.

56 L. Salvati, L. E. Makovsky, J. M. Stencel, F. R. Brown and D. M. Hercules, *J. Phys. Chem.*, 1981, **85**, 3700–3707.

57 G. C. Silva, D. Qian, R. Pace, O. Heintz, G. Caboche, E. Santillan-Jimenez and M. Crocker, *Catalysts*, 2020, **10**, 91.

58 R. Loe, Y. Lavoignat, M. Maier, M. Abdallah, T. Morgan, D. Qian, R. Pace, E. Santillan-Jimenez and M. Crocker, *Catalysts*, 2019, **9**, 123.

59 A. Veses, M. Aznar, I. Martínez, J. D. Martínez, J. M. López, M. V. Navarro, M. S. Callén, R. Murillo and T. García, *Bioresour. Technol.*, 2014, **162**, 250–258.

60 M. C. Alvarez-Galvan, G. Blanco-Brieva, M. Capel-Sanchez, S. Morales-delaRosa, J. M. Campos-Martin and J. L. Fierro, *Catal. Today*, 2018, **302**, 242–249.

61 A. Srifa, K. Faungnawakij, V. Itthibenchapong, N. Viriya-empikul, T. Charinpanitkul and S. Assabumrungrat, *Bioresour. Technol.*, 2014, **158**, 81–90.

62 Y. Yang, Q. Wang, X. Zhang, L. Wang and G. Li, *Fuel Process. Technol.*, 2013, **116**, 165–174.

63 P. Šimáček, D. Kubička, G. Šebor and M. Pospíšil, *Fuel*, 2009, **88**, 456–460.

64 A. Ramesh, P. Tamizhdurai and K. Shanthi, *Renewable Energy*, 2019, **138**, 161–173.

65 S. Khan, A. N. Kay Lup, K. M. Qureshi, F. Abnisa, W. M. A. Wan Daud and M. F. A. Patah, *J. Anal. Appl. Pyrolysis*, 2019, **140**, 1–24.

66 X. Li, X. Luo, Y. Jin, J. Li, H. Zhang, A. Zhang and J. Xie, *Renewable Sustainable Energy Rev.*, 2018, **82**, 3762–3797.

67 L. Chen, H. Li, J. Fu, C. Miao, P. Lv and Z. Yuan, *Catal. Today*, 2016, **259**, 266–276.

68 V. A. Yakovlev, S. A. Khromova, O. V. Sherstyuk, V. O. Dundich, D. Y. Ermakov, V. M. Novopashina, M. Y. Lebedev, O. Bulavchenko and V. N. Parmon, *Catal. Today*, 2009, **144**, 362–366.

69 A. Srifa, R. Kaewmeesri, C. Fang, V. Itthibenchapong and K. Faungnawakij, *Chem. Eng. J.*, 2018, **345**, 107–113.

70 J. Liu, C. Liu, G. Zhou, S. Shen and L. Rong, *Green Chem.*, 2012, **14**, 2499–2505.

71 E. Santillan-Jimenez, T. Morgan, J. Shoup, A. E. Harman-Ware and M. Crocker, *Catal. Today*, 2014, **237**, 136–144.

72 J. Gao, Y. Wang, Y. Ping, D. Hu, G. Xu, F. Gu and F. Su, *RSC Adv.*, 2012, **2**, 2358–2368.

73 T. Morgan, E. Santillan-Jimenez, A. E. Harman-Ware, Y. Ji, D. Grubb and M. Crocker, *Chem. Eng. J.*, 2012, **189–190**, 346–355.

74 N. Asikin-Mijan, N. A. Rosman, G. AbdulKareem-Alsultan, M. S. Mastuli, H. V. Lee, N. Nabihah-Fauzi, I. M. Lokman, F. A. Alharthi, A. A. Alghamdi, A. A. Aisyahi and Y. H. Taufiq-Yap, *Process Saf. Environ. Prot.*, 2020, **142**, 336–349.

75 M. R. Nimkarde and P. D. Vaidya, *Energy Fuels*, 2016, **30**, 3107–3112.

76 N. D. Charisiou, G. I. Siakavelas, B. Dou, V. Sebastian, S. J. Hinder, M. A. Baker, K. Polychronopoulou and M. A. Goula, *Catalysts*, 2019, **9**, 411.

77 G. Goula, G. Botzolaki, A. Osatiashtiani, C. M. Parlett, G. Kyriakou, R. M. Lambert and I. V. Yentekakis, *Catalysts*, 2019, **9**, 541.

78 K. Polychronopoulou, N. D. Charisiou, G. I. Siakavelas, A. A. Alkhoori, V. Sebastian, S. J. Hinder, M. A. Baker and M. A. Goula, *Sustainable Energy Fuels*, 2019, **3**, 673–691.

79 K. N. Papageridis, N. D. Charisiou, S. Douvartzides, V. Sebastian, S. J. Hinder, M. A. Baker, S. AlKhoori, K. Polychronopoulou and M. A. Goula, *Renewable Energy*, 2020, **162**, 1793–1810.

80 M. Velasquez, C. Batiot-Dupeyrat, J. Gallego, J. J. Fernández and A. Santamaria, *Diamond Relat. Mater.*, 2016, **70**, 105–113.

81 M. Velasquez, C. Batiot-Dupeyrat, J. Gallego and A. Santamaria, *Diamond Relat. Mater.*, 2014, **50**, 38–48.

82 F. Gholizadeh, A. Izadbakhsh, J. Huang and Y. Zi-Feng, *Microporous Mesoporous Mater.*, 2021, **310**, 110616.

83 V. Alcalde-Santiago, A. Davó-Quiñonero, D. Lozano-Castelló, A. Quindimil, U. De-La-Torre, B. Pereda-Ayo, J. A. González-Marcos, J. R. González-Velasco and A. Bueno-López, *ChemCatChem*, 2019, **11**, 810–819.

84 J. H. Lehman, M. Terrones, E. Mansfield, K. E. Hurst and V. Meunier, *Carbon*, 2011, **49**, 2581–2602.

85 N. D. Charisiou, G. Siakavelas, K. N. Papageridis, A. Baklavaridis, L. Tzounis, G. Goula, I. V. Yentekakis, K. Polychronopoulou and M. A. Goula, *Front. Environ. Sci.*, 2017, **5**, 66.

86 O. Padilla, J. Gallego and A. Santamaría, *Diamond Relat. Mater.*, 2018, **86**, 128–138.

87 A. V. Ramya, A. N. Mohan and B. Manoj, *Mater. Sci.-Pol.*, 2016, **34**, 330–336.